# Theory for the ultrafast dynamics of excited clusters: interplay between elementary excitations and atomic structure

**M.E. Garcia**[*], **H.O. Jeschke, I. Grigorenko, K.H. Bennemann**

Institut für Theoretische Physik der Freien Universität Berlin, Arnimallee 14, 14195 Berlin, Germany

**Abstract.** We present a theoretical study of the short-time relaxation of clusters in response to ultrafast excitations using femtosecond laser pulses. We analyze the excitation of different types of clusters ($Hg_n$, $Ag_n$, $Si_n$, $C_{60}$ and $Xe_n$) and classify the relaxation dynamics in three different regimes, depending on the intensity of the exciting laser pulse.

For low-intensity pulses ($I < 10^{12}\,W/cm^2$) we determine the time-dependent structural changes of clusters upon ultrashort ionization and photodetachment. We also study the laser-induced non-equilibrium fragmentation and melting of $Si_n$ and $C_{60}$ clusters, which occurs for moderate laser intensities, as a function of the pulse duration and energy.

As an example for the case of high intensities ($I > 10^{15}\,W/cm^2$), the explosion of clusters under the action of very intense ultrashort laser fields is described.

**PACS:** 36.40.-c; 31.70.Hq; 32.80.Fb

Since the development of femtosecond spectroscopy [1], much attention has been paid to the investigation of ultrafast processes in atoms, molecules and small clusters. One of the reasons for this is that this technique makes it possible to address a fundamental problem in the physics of small clusters and molecules, which is the description of relaxation mechanisms in the sub-picosecond time domain. The ultrafast dynamics of a cluster is usually induced by an ultrashort laser pulse which excites the cluster, abruptly bringing it to a non-equilibrium state.

Both the excitation process and the subsequent relaxation dynamics depend on the intensity and duration of the exciting laser pulse. For low intensities, the laser pulse usually cannot excite more than one electron (or collective state) per cluster. To this category of excitations belong the ultrafast single ionization and single photodetachment of the cluster. These processes already lead to strong time-dependent structural changes (including evaporation of atoms).

When the laser intensity reaches moderate values ($I \sim 10^{10}$–$10^{12}\,W/cm^2$), more than one excitation can be produced in the cluster. This means that more energy can be pumped into the cluster, which leads to an enhancement of the bond-breaking processes during the relaxation.

Finally, for very high intensities of the laser pulses ($I > 10^{15}\,W/cm^2$), each cluster absorbs many photons, and qualitatively new phenomena appear, like multiple ionization of core electrons, emission of X-rays, relativistic effects, etc.

In the following we briefly review the open questions in the different intensity regimes and present the goals of this paper.

### A. Low intensities

*Ultrafast ionization.* In recent years, many different pump& probe experiments have been performed to study the ultrafast dynamics of excited and ionized clusters [2–8]. In those experimental studies where the fragmentation behavior is investigated [2, 3, 7], results are usually interpreted in terms of master equations, assuming constant decay probabilities. It is unclear whether this constant-rate assumption is valid for such non-equilibrium processes. An important problem is also whether the ionization-induced fragmentation dynamics is sensitive to the initial conditions, like the temperature or the thermodynamic state (solid-like or liquid-like) of the cluster.

In this paper we present a theoretical description of the ionization-induced fragmentation dynamics of small van der Waals clusters, and show that the ultrafast dynamics opens a possibility of the experimental observation of phase transitions in small systems.

As we assume low laser intensities, we shall consider only fragmentation after single ionization. It is well known that vertical ionization of van der Waals clusters induces dramatic changes in their electronic structure [9]. After ionization, the electronic structure is governed by polarization effects, by the kinetic energy of the positive charge, and by dipole–dipole interactions [10], which result in strong attractive interactions between the atoms, in contrast to the weak van der Waals interactions present before ionization. Therefore, van der Waals

---

[*] Corresponding author. (E-mail: garcia@physik.fu-berlin.de)

aggregates are particularly suitable systems for the study of energy-transfer processes after electronic excitation. In fact, fragmentation of rare-gas clusters upon single ionization has been experimentally observed [11, 12].

Small $Hg_n$ clusters ($n \leq 13$) are van der Waals-bonded [24–26]. Ionization produces in these clusters the same changes (polarization and hole delocalization) as in rare-gas clusters, leading to the same size-dependence of the ionization potentials [10, 26, 27]. In recent pump&probe experiments a rapid fragmentation of $Hg_n$ clusters within the first picoseconds after excitation in a Rydberg state was observed [3]. On the other hand, in conventional photo-ionization experiments on large $Hg_n$ clusters, which exhibit covalent or metallic bonding character, no fragmentation after single ionization has been observed [27]. In this paper we show that for small $Hg_n$ clusters ($n \leq 13$) fast fragmentation, consisting mainly of emission of neutral atoms, is possible after single ionization produced by an ultrashort laser pulse.

*Ultrafast photodetachment.* An interesting example for time-dependent bond breaking and bond formation is given by the short-time dynamics of $Ag_3$ clusters formed by ultrashort photodetachment of $Ag_3^-$. Recently, this dynamics has been monitored in a pump&probe experiment performed on mass-selected $Ag_3^-$ clusters [6].

In this experiment the initially negatively charged clusters were neutralized through photodetachment by the pump pulse and after a delay ionized by the probe pulse in order to be detected. Due to the large differences in the equilibrium geometries of linear $Ag_3^-$ [13], and obtuse isosceles triangular $Ag_3$ [14], the ultrashort photodetachment process puts the neutralized trimer in an extreme non-equilibrium situation. As a consequence, a structural relaxation process occurs.

The experimental signal of the $Ag_3^+$ yield was measured as a function of the delay time $\Delta t$ and the frequency of the laser pulses. For a frequency slightly above the ionization potential of $Ag_3$, a sharp rise of the signal is observed at approximately 750 fs [6]. After a maximum is reached, there is a saturation of the signal, which then remains constant for at least 100 ps, which is the longest time delay used in the experiment [6]. New features appear for higher frequencies. Again the signal increases sharply, reaches a maximum and then decreases to a constant value. A preliminary interpretation of these results was given using the Franck–Condon principle [6]. The first laser pulse creates a neutral linear silver trimer which begins to bend, passes through the obtuse isosceles triangle equilibrium geometry of the neutral $Ag_3$, and comes to a turning point near the equilateral equilibrium geometry of the positive ion [14]. After rebounding, the neutral trimers start pseudorotating through their three equivalent obtuse isosceles equilibrium geometries.

This would explain the saturation behavior of the signal. However, this would mean that the pseudorotations have an extremely long mean lifetime. This seems improbable to us. Furthermore, it is not clear why the signal changes as a function of the frequency of the laser pulse.

In this paper we perform a theoretical analysis of the physics underlying the ultrafast dynamics of $Ag_3$ clusters produced by photodetachment. In particular, we analyze the time evolution of the ionization potential and the dependence of the dynamics on the initial temperature of the clusters. We show that the experimental results can be explained using a physical picture which can be generally applied to other ultrashort-time processes.

## B. Moderate intensities

The phenomenon of laser-induced phase transitions in semiconductors has attracted considerable attention during recent years [15–17]. In most studies a very fast melting of the crystalline structure is observed [15, 16], with a time scale of a few hundred femtoseconds. The question of whether other kinds of laser-induced transitions, like structural transformations and changes in the bond character, are accessible by suitable adjustment of the laser parameters, still remains open.

To address the problem of laser-induced melting of bulk silicon, for instance, different theoretical approaches have been used [18–20]. These methods assume that the volume of the system remains constant throughout the relaxation process. Therefore, the lattice is not allowed to expand. In bulk matter this assumption might be reasonable for the description of non-equilibrium melting, but fails to describe laser-induced transitions involving volume changes. For that reason these methods cannot be applied to small clusters.

In the above-mentioned theoretical investigations the duration $\tau$ of the exciting pulse is not explicitly taken into account. A sudden excitation of the system is assumed (zero duration).

Finite pulse durations are of fundamental importance, since they induce interesting physical processes which are different from those involved in the limiting cases $\tau \to 0$ (sudden excitation) and $\tau \to \infty$ (adiabatic excitation). The role of the pulse duration on the laser-induced dynamics has been shown to be essential for optical control of microscopic processes (pump&control). In the field of atomic and molecular physics, first coherent control scenarios have already been investigated [21].

One of the goals of the present paper is to perform a theoretical study of the laser-induced ultrashort-time dynamics of small $Si_n$ as a function of the duration of the exciting laser pulse and without any constraints on the volume of the system.

In the study of the relaxation dynamics, we also deal with the question of under which conditions the clusters undergo a transition to a liquid-like phase, as was observed in crystalline semiconductors.

We also show that the laser excitation can lead to multiple bond breaking in the clusters and study the fragmentation dynamics as a function of the laser parameters. Fragmentation of silicon clusters upon excitation with femtosecond laser pulses was observed recently by G. Gerber and coworkers [22]. They observed that femtosecond pulses lead to a much stronger fragmentation of the cluster than nanosecond pulses. The same group has performed time-resolved experiments, in which the concentration of $Si_n^+$ clusters excited by the pump pulse was recorded as a function of time after excitation. The resulting curves show an exponential decrease for all cluster sizes with time constants between 2 ps and 9 ps. The decay times are shown to be dependent on laser intensity.

In this paper we give a qualitative theoretical explanation of why short pulses may lead to more fragmentation than long pulses.

We also analyze the laser-induced ultrafast dynamics of a large $Si_n$ cluster ($n = 200$), and of a $C_{60}$ cluster in response to laser pulses of finite duration and moderate intensities.

### C. High intensities

Recent experiments on clusters irradiated by strong laser pulses (intensity $I > 10^{14}$ W/cm$^2$) have revealed phenomena not previously seen in experiments on atoms and small molecules: generation of highly charged atomic ions (ionic charge $q > 30\,e$, with $e$ the elementary charge) [28–30, 32–34], emission of intense X-rays by 'hollow' atoms [35] and by hot plasmas [32], coherent high-harmonic radiation [36], and electrons [31] and ions [31, 37] emitted with kinetic energies in excess of 100 keV. In the case of strong ionization leading to highly charged fragments, interesting effects involving characteristic time scales have also been observed [34].

The phenomena induced by very intense pulses on clusters differ qualitatively from those observed in atoms and molecules, due to the presence of collective effects. Clusters are also interesting subjects of study because the different effects can be analyzed as a function of the size.

In this paper we present a model to describe explosion of a cluster after interaction with short intense laser pulses by simultaneous solution of the quantum-mechanical equation of motion for the electrons and the classical equations of motion for the nuclei. We will show that the interesting features of the explosion of clusters induced by very intense laser pulses result from the coupling between the motion of electrons and nuclei under the influence of the external laser field.

This paper is organized as follows. In Sect. 1 we outline the different theoretical approaches that we used to address the different problems for low, moderate and high laser intensities. In Sect. 2 we present a summary of our most important results. Finally, in Sect. 3 we present a general and brief summary of our results.

## 1 Theory

In this section we describe the theoretical methods used to treat the laser-induced ultrafast dynamics of clusters upon excitation by femtosecond pulses having low, moderate and high intensities. For the case of low intensities we assume a sudden excitation of the system (zero pulse duration), whereas for moderate and high intensities we consider explicitly the envelope and duration of the laser pulse.

### 1.1 Low laser intensities. Pulses of zero duration

We consider two problems related to the regime of low intensities: ultrafast ionization of small $Hg_n$ clusters and ultrafast photodetachment of $Ag_3^-$.

### 1.1.1 Response of $Hg_n$ clusters to ultrafast ionization.

We combine a self-consistent electronic theory and molecular-dynamics simulations in the Born–Oppenheimer approximation. Usually, for MD simulations of neutral van der Waals clusters, parameterized pair potentials are used [23]. However, this description is no longer valid when these clusters

become ionized. As a result of the competition between the delocalization energy of the positive charge (hole) and the polarization energy of the cluster [9, 10, 39, 40], only a partial delocalization of the hole within a sub-cluster of $m_s$ atoms (ionic core) occurs [10, 41][1]. The rest of the atoms remain neutral and can be polarized. Thus, in order to account for the time-dependent changes of the charge and dipole distributions during the relaxation following ionization, the potential-energy surface (PES) must be determined self-consistently. A quite reasonable description of the ground state of these systems is achieved by assuming the ionic sub-cluster to be a dimer ($m_s = 2$) [41]. Thus, we use the dimer-core approximation, which enormously simplifies the calculations. This model, which just imposes a constraint on the charge distribution of the cluster ion, has also been used, in combination with different electronic theories, to calculate cohesive energies and ionization potentials of ionized rare-gas clusters [10, 42–44].

Hence, after imposing this constraint for the charge distribution, the system is described by the Hamiltonian [10, 39, 40]

$$H = H_{vdW} + H_{core} + H_{Q-P} + H_{P-P}, \qquad (1)$$

where $H_{vdW}$, $H_{core}$, $H_{Q-P}$, and $H_{P-P}$ describe, respectively, the van der Waals interactions in the whole cluster, the hole hopping within the ionic core, the inter-atomic charge–dipole interactions between the ionic core and the neutral rest, and the dipole–dipole interactions between the $n - 2$ neutral atoms. The many-body Hamiltonian $H$ can be approximated by an effective single-hole Hamiltonian by writing the charge and dipole operators as $P_k = \langle P_k \rangle + \delta P_k$ and $Q_l = \langle Q_l \rangle + \delta Q_l$, and neglecting terms containing charge–dipole fluctuations [10, 39, 40]. The resulting effective Hamiltonian can be easily diagonalized, and for $m = 2$ one obtains a closed expression for the electronic ground-state energy of the ionized cluster [39, 40, 45] $E(r_1, \ldots, r_n)$. The function $E(r_1, \ldots, r_n)$ depends on the atomic coordinates, and defines (within the Born–Oppenheimer approximation) a PES for the motion of the atoms.

In order to write and solve the equations of atomic motion we have to calculate the forces acting on the atoms. The $\mu$ component of the force acting on a given atom $i$ is given by

$$F_j^\mu = -\frac{\partial E(r_1, \ldots, r_n)}{\partial r_j^\mu}. \qquad (2)$$

For each set of atomic coordinates (i.e., for each MD-step) the charge and dipole distributions and consequently the energy $E(r_1, \ldots, r_n)$ have to be solved self-consistently. Note that the energy $E(r_1, \ldots, r_n)$ cannot be described as a sum of pair potentials [39, 40]. Finally, we integrate the equations of motion for the atomic coordinates $r_j$ and the corresponding velocities $\dot{r}_j$ using the Verlet algorithm (in velocity form [48]) as

$$r_j(t_i) = r_j(t_{i-1}) + \Delta t\, \dot{r}_j(t_i) + \frac{1}{2m}(\Delta t)^2 F_j(t_{i-1}),$$

---

[1] All-electron calculations support the occurrence of a dimer or a trimer, the energy difference being small.

$$\dot{\boldsymbol{r}}_j(t_i) = \dot{\boldsymbol{r}}_j(t_{i-1}) + \frac{1}{2m}\Delta t \left[ \boldsymbol{F}_j(t_{i-1}) + \boldsymbol{F}_j(t_i) \right], \qquad (3)$$

where $m$ is the mass of the Hg atom, and $\Delta t$ the time step for the integration.

Note that for the analytical calculation of the forces by using (2) we have to determine the derivatives of the charge and dipole distributions with respect to the atomic coordinates. This is done self-consistently for each time step.

In the following, we assume that the width of the ionizing laser pulse is negligible compared to the time scale of the nuclear motion. In other words, we consider the action of an external field $\hat{I}(t)$ of the form $\hat{I}(t) = \delta(t - t_0) I_0 h_d^+ p_n^+$, where $t_0$ represents the ionization time. $h_d^+$ is an operator which creates a hole in the ground-state dimer core and $p_n^+$ creates the $n-2$ induced dipole moments in the neutral atoms surrounding the ionic core.

*1.1.2 Response of* $Ag_3^-$ *to ultrafast photodetachment.* In order to determine the PES needed for the MD simulations, we start from a Hamiltonian of the form $H = H_{TB} + 1/2 \sum_{i \neq j} \phi(\boldsymbol{r}_{ij})$, where $H_{TB}$ is a tight-binding Hamiltonian, and $\phi(\boldsymbol{r}_{ij})$ refers to the repulsive potential between the atomic cores $i$ and $j$. In $H_{TB}$, the orbitals $\alpha = 5s, 5p_x, 5p_y, 5p_z$ are taken into account. For the distance-dependence of the hopping elements and the repulsive potential we use the functional form proposed in [46]. By diagonalizing $H_{TB}$ (taking into account the angular dependence of the hopping elements [47]), and summing over the occupied states, we calculate as a function of the atomic coordinates the attractive parts of the electronic ground-state energies $E_{attr}^-$ and $E_{attr}^0$ of $Ag_3^-$ and $Ag_3^0$, respectively. Then, by adding the repulsive part of $H$ we obtain the PES, which we need to perform the MD simulations. In order to determine the forces acting on the atoms we make use of the Hellman–Feynman theorem. The parameters of $H$ are determined in the following way. The on-site energies were obtained from atomic data [49]. We fit the parameters $V_{\alpha\beta}$ and the potential $\phi(\boldsymbol{r}_{ij})$ in order to reproduce the equilibrium bond lengths of the silver dimers $Ag_2^-$, $Ag_2$ and $Ag_2^+$ obtained by effective core potential–configuration interaction calculations [13, 14]. We assumed the hopping elements $V_{\alpha\beta}$ to fulfill Harrison's relations [50]. The best fit was obtained by the following parameters: $V_{sp} = 0.954$ eV, $r_c = 4.33$ Å, $n_c = 2$, $m = 5.965$ and $A = 0.605$ eV, where $r_c$ and $n_c$ refer to the cutoff radius and exponent, whereas $m$ and $A$ stand for the exponent and strength of the repulsive potential $\phi(\boldsymbol{r}_{ij})$ [46]. Using these parameters, we have calculated the vibrational frequencies of the dimers, which compare reasonably well with the experimental values [51] and quantum-chemical calculations [13, 14]. Then, we determined the equilibrium geometries of the ground states of the silver trimers $Ag_3^-$, $Ag_3$ and $Ag_3^+$, which again yielded excellent agreement with the all-valence-electron calculations of [13] and [14].

The MD simulations are performed by applying the Verlet algorithm in its velocity form. We used a time step of $\Delta t = 0.05$ fs. This ensures an energy conservation up to $10^{-6}$ eV after $10^5$ time steps. The equilibrium structures were obtained by performing simulated annealing. Starting with the equilibrium geometry of $Ag_3^-$, we generate an ensemble of approximately 1000 clusters characterized by the ensemble temperature $T$, defined as the time average of the kinetic energy for a long trajectory ($\sim 10^6$ time steps) [23]. We then model the action of the pump-laser pulse, which in the experiment performs the photodetachment and thus initiates the strong response of the now neutral $Ag_3$ clusters, by removing the additional electron of every $Ag_3^-$ cluster in the ensemble at the same time. This corresponds to the action of a $\delta$-shaped laser pulse and thus only approximates the situation in the experiment [6], where 90 fs pulses are used, but as the experimental signal only develops on a time scale of $\Delta t \simeq 750$ fs, the approximation seems justified. After photodetachment, the evolution of the cluster ensemble on the PES of neutral $Ag_3$ is calculated.

*1.2 Moderate laser intensities. Pulses of finite duration*

*1.2.1 Relaxation dynamics of* $Si_n$ *clusters and* $C_{60}$. In the case of small $Si_n$ clusters we assume that the time scales for the electron and atomic motions can be separated. This assumption is justified by experimental results on bulk materials [52, 53], which indicate that the relaxation time for the electrons is extremely small ($\sim 10$ fs) compared with the time scale for the motion of the atoms. Since we are interested in structural changes with time scales which are larger than 10 fs, even the drastic assumption of separated time scales should work reasonably. As a consequence of this separation of time scales we can study the dynamics of the cluster in the adiabatic limit and consider that electrons thermalize immediately after excitation. On this basis we can then treat the atomic motion in the Born–Oppenheimer approximation.

Note that the approximation of separable time scales for atoms and electrons was also used by C.A. Ullrich et al. to treat the ultrafast dynamics of electrons in highly excited metallic clusters [54].

In a first step we calculate the electronic energy of the ground-state configuration by diagonalization of a tight-binding Hamiltonian. The action of the laser is then considered by inducing electronic transitions from occupied to unoccupied TB-states. Since we assume an instantaneous thermalization of the electrons, the occupation of the excited states is given by a Fermi–Dirac distribution determined by the laser-induced temperature $T_{el}$ [55]. The total energy of the excited electronic system is a function of atomic coordinates. The forces governing the atomic motion are obtained using the Hellmann–Feynman theorem.

For the microscopic description of $Si_n$ clusters we use a Hamiltonian of the form $H_{el} = H_{TB} + \sum_{i<j}^{N} \Phi_{rep}(R_{ij})$ built up by an attractive term, derived in the tight-binding approximation, and a potential accounting for the core–core repulsion.

The total electronic energy of the $Si_n$ clusters for a given electronic configuration described by the set of occupations $\{n_k\}$ of the tight-binding eigenstates is obtained by diagonalizing the tight-binding Hamiltonian and evaluating the expression:

$$E(\{R_j\}) = \sum_k 2n_k < \Phi_k | H_{TB} | \Phi_k > + E_{rep} + E_0 N_{at}. \qquad (4)$$

The attractive term is a sum over the eigenvalues $\varepsilon_k$ of filled tight-binding states, $E_{rep}$ the potential energy due to the core–core repulsion and $E_0 N_{at}$ the energy of $N_{at}$ isolated Si atoms.

The factor 2 arises because each state is occupied by two electrons with opposite spin. The total electronic energy depends, through the Hamiltonian $H_{TB}$ and the energy $E_{rep}$, on the atomic coordinates ($\{R_j\}$), thus providing the potential-energy surface which determines the atomic motion.

As we mentioned above, we assume that the laser produces thermalized electron–hole pairs [55, 56]. Thus, the occupation number of the tight-binding state $\varepsilon_k$ is then given by a Fermi–Dirac distribution $n_k(T_{el}) = [\exp(\beta(\varepsilon_k - \mu)) + 1]^{-1}$, where $\beta = 1/k_B T_{el}$. The chemical potential $\mu$ can be determined by the constraint that the number of electrons in the system is constant: $N_{el} = \sum_k n_k = 4N_{at}$. To get a better comparison with experimental parameters, it is convenient to characterize the laser by the energy it transfers to the electrons, which are assumed to be initially at $T_{el} = 0$. This energy is referred to as the total absorbed energy $E_{abs}$[2]. The energy absorbed by the cluster until the time $t$ can be written as $\Delta_{abs}(t) = E(T_{el}(t)) - E(T_{el} = 0)$. Now, the absorbed energy, assuming that laser energy flows into the system following a Gauss profile, is also given by

$$\Delta_{abs}(t) = I_0 \int_0^t dt' \exp\left[\frac{-(t' - t_0)^2 4\ln 2}{\tau^2}\right], \qquad (5)$$

where $\tau$ is the pulse duration. The intensity of the laser pulse $I_0$ is related to the total absorbed energy $\Delta_{abs}(t \to \infty)$ by $I_0 = 4\Delta_{abs}(t \to \infty)\sqrt{\ln 2/\pi}/\tau$. From this equation we determine $T_{el}(t)$. Given this quantity we are now able to determine the time-dependent level occupations, the time-dependent energy, and the forces acting on the atoms, and therefore to solve the equations of motion (for more details see [55]).

For the study of large Si$_n$ clusters and C$_{60}$ we have improved our model in order to take into account electron-thermalization effects by the solution of a Bolzmann-like rate equation. Thus, the constraint of zero relaxation time for the electrons is relaxed (for more details see [57]).

### 1.3 High laser intensities. Coulomb explosion

In this model we consider that all particles move only in one spatial dimension. This approximation has been applied extensively in the treatment of strong laser pulse interaction with atoms [58] and small molecules [59] and clusters [60]. It should be mentioned that precise time-dependent Kohn–Sham calculations, like those performed by Reinhard and coworkers [38], cannot be applied to the study of multiple ionization (ionization of core electrons). The numerical integration of the equations of motion for all electrons in a large cluster in a very dense space lattice cannot be presently achieved.

In the following we use atomic units ($\hbar = m = e = 1$). We characterize all electrons in the Xe$_N$ cluster by the electronic density $\varrho(x, t) = |\psi(x, t)|^2$, where $\psi(x, t)$ results from the Schrödinger equation:

$$i\hbar \frac{\partial \psi}{\partial t} = (\hat{\mathcal{H}}_{el} + \hat{V}_{int}^{e-i} + \hat{\mathcal{H}}_{field})\psi, \qquad (6)$$

where the attraction of the nuclei $\hat{V}_{int}^{e-i}$ is given by:

$$\left\langle \psi \left| \hat{V}_{int}^{e-i} \right| \psi \right\rangle = -Q \sum_{i=1}^N \int dx \frac{|\psi(x, t)|^2}{\sqrt{(x - R_i(t))^2 + a^2}}. \qquad (7)$$

$R_i(t), i = 1, \ldots, N$ are the current positions of the nuclei, $Q = 54$ is the atomic number of xenon and $a$ is a smoothing parameter. We use the standard smoothing of the Coulomb potential, which retains the long-range interaction while eliminating the singularity at $x = 0$. We use parameter values $a = c = 2.5$ and $b = 3.4$, which yield an equilibrium internuclear separation of 0.44 nm for a Xe$_2$ molecule. Interaction with external radiation $\hat{\mathcal{H}}_{field}$ is

$$\left\langle \psi \left| \hat{\mathcal{H}}_{field} \right| \psi \right\rangle = \int dx |\psi(x, t)|^2 E_{field}(t) \sin(\omega t)x. \qquad (8)$$

Here $E_{field}(t)$ is the envelope of the laser pulse with frequency $\omega$. The electronic part of the Hamiltonian $\hat{\mathcal{H}}_{el}$ can be written as

$$\hat{\mathcal{H}}_{el} = -\frac{\hbar^2}{2m}\nabla^2 + \hat{\mathcal{H}}_{int}^{e-e} + \hat{\mathcal{H}}_{xc}. \qquad (9)$$

This part includes the kinetic term, the Coulomb repulsion $\hat{\mathcal{H}}_{int}^{e-e}$ between electrons

$$\left\langle \psi \left| \hat{\mathcal{H}}_{int}^{e-e} \right| \psi \right\rangle = \frac{1}{2} \int dx \int dx' \frac{|\psi(x, t)|^2 |\psi(x', t)|^2}{\sqrt{(x - x')^2 + b^2}}, \qquad (10)$$

and the exchange-correlation $\hat{\mathcal{H}}_{xc}$ term in local-density approximation:

$$\left\langle \psi \left| \hat{\mathcal{H}}_{xc} \right| \psi \right\rangle = -\frac{3}{4}\left(\frac{3}{\pi}\right)^{\frac{1}{3}} \int dx |\psi(x, t)|^{\frac{8}{3}}. \qquad (11)$$

The Hamiltonian $\hat{\mathcal{H}}_{ion}$ for the nuclei is

$$\hat{\mathcal{H}}_{ion} = \sum_{i=1}^N \frac{P_i^2}{2M} + \frac{1}{2} \sum_{i \neq j}^N \frac{Q^2}{\sqrt{(R_i - R_j)^2 + c^2}} + \hat{V}_{int}^{e-i}$$
$$- \sum_{i=1}^N Q E_{field}(t) \sin(\omega t) R_i, \qquad (12)$$

containing again a kinetic part, a Coulomb repulsion between nuclei, the attraction to the electrons and the interaction with an external laser field. The equations of motion for the nuclei are simply a system of Newton's equations:

$$M \frac{\partial^2 R_i}{\partial t^2} = F_i, \qquad (13)$$

where $M$ is the mass of a nucleus and the forces acting on the nuclei are given by

$$F_i = -\frac{\partial E}{\partial R_i} = -\frac{\partial \left\langle \psi | \hat{\mathcal{H}}_{ion} | \psi \right\rangle}{\partial R_i}. \qquad (14)$$

The time evolution of the cluster is obtained by integrating in a parallel way the Schrödinger equation for the wave function $\psi(x, t)$ and the classical equations of motion for the nuclear coordinates. The Schrödinger equation is integrated with the help of the split-operator technique.
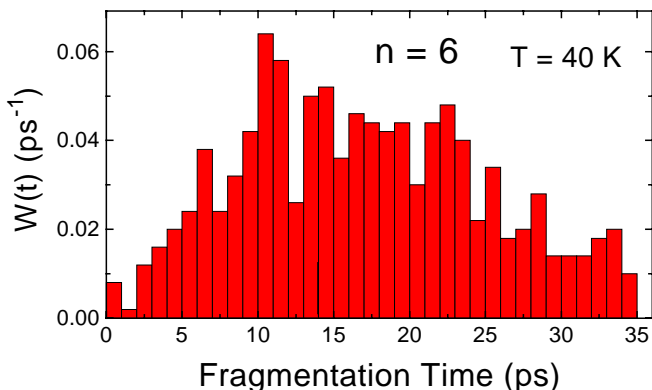
## 2 Results

### 2.1 Low laser intensities. Pulses of zero duration

*2.1.1 Response of* Hg$_n$ *clusters to ultrafast ionization.* On the basis of our model presented in Sect. 1.1.1 the main physics of the dynamics described by this theory can be visualized as follows. Through the ionization process, the Lennard–Jones PES of the neutral cluster is switched to the PES of the ionized cluster. The binding energy of the ionized cluster is much larger than that of the neutral cluster (already the delocalization energy of the hole is about 1.4 eV) and the equilibrium inter-atomic distances are considerably smaller. At the moment of ionization the cluster structure is that of the neutral state, which is very different from the ground-state configuration of the ionized cluster. Thus, a relaxation process takes place in which the excess energy $\delta E$ (which is approximately the difference between the binding energies of the ionized and neutral clusters) is redistributed among the different atomic degrees of freedom.

As a general result we obtained ionization-induced fragmentation for all cluster sizes under study ($3 \leq n \leq 13$) at all initial temperatures considered. Note, however, that within the time window considered (0 to 100 ps) a considerable fraction of the clusters did not fragment. The neutral fragments obtained were mainly monomers. The probability for emission of neutral dimers turned out to be small.

In order to describe real experimental conditions, we performed simulations at non-zero initial temperature. Thus, we obtained, for each cluster size and each initial temperature, a distribution of fragmentation times given by the number of clusters whose fragmentation occurs at $\tau_F$ [39, 40]. In Fig. 1 we show the normalized fragmentation-time distribution, $W(\tau_F)$, calculated for Hg$_6^+$ clusters with an initial temperature of $T = 40$ K. The fragmentation histogram $W(t_F)$ has been determined as follows. For each member $i$ of the temperature ensemble we obtained $t_F^i$ from the MD simulations after ionization. Then we calculated the quantity $\sum_i \delta(t_F - t_F^i)$ and integrated it within finite time intervals. Note that one can interpret the function $W(t)$ as the probability of fragmentation per unit time.

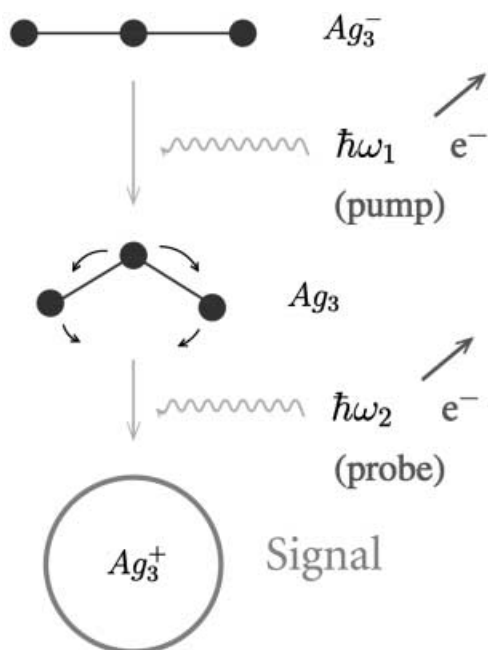For low temperatures, the calculated $W(t)$ and the corresponding values of the average fragmentation time $\langle \tau_F \rangle$ show only a weak temperature dependence. However, we obtain a remarkable change in $W(t)$ in a temperature range which can be related to the solid-like to liquid-like transition of neutral clusters. This indicates a correlation between the energy-transfer mechanisms after ionization and the thermodynamic state of the cluster before ionization.

For a more quantitative analysis of the temperature dependence of the average fragmentation times we have calculated the root-mean-square (rms) bond-length fluctuation $\delta$ [40]. For bulk material and in clusters, $\delta$ shows typically a sharp increase at the temperature corresponding to the solid–liquid transition, consistent with the Lindemann criterion [23]. In Fig. 2a,b the temperature dependence of $\delta$ is shown for Hg$_n$ clusters ($n = 3, 13$). For $n = 3$ and 13, $\delta$ clearly shows a jump [45]. In Fig. 2 we also show the temperature behavior of the inverse fragmentation time $\langle \tau_F \rangle^{-1}(T)$. Clearly, there is a remarkable sensitivity of the average fragmentation times to the melting dynamics. Note that $\delta(T) \propto \langle \tau_F \rangle^{-1}(T)$. Such a correlated temperature dependence can be understood as follows. Fragmentation occurs on an average after a certain (incomplete) thermalization process. Thus, the distribution of the excess energy $\delta E$ among the different degrees of freedom leads to a homogeneous weakening of the bonds. This means that atoms (fragments) are emitted from a liquid-like cluster. If the cluster was in a solid-like state before ionization, part of the relaxation energy $\delta E$ has to be used first as latent heat. Only after melting can fragmentation occur. As a consequence, the mean fragmentation times are smaller for initially liquid clusters.
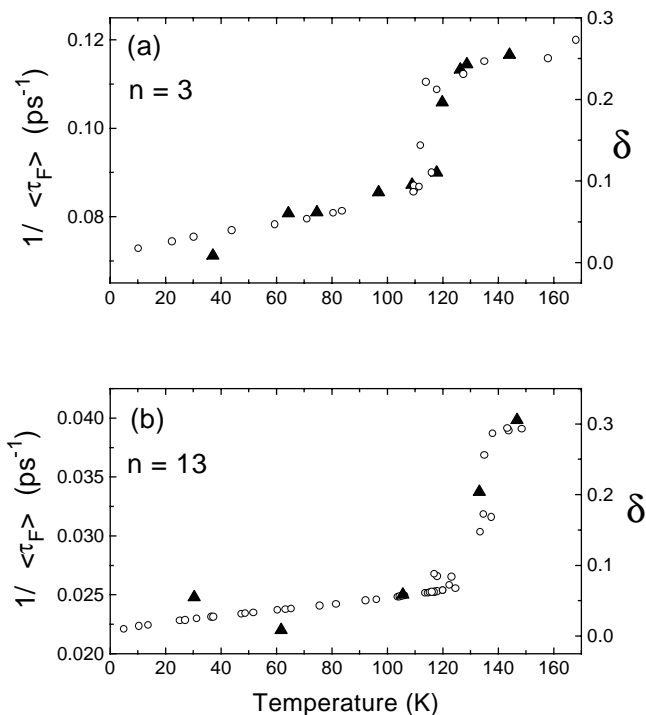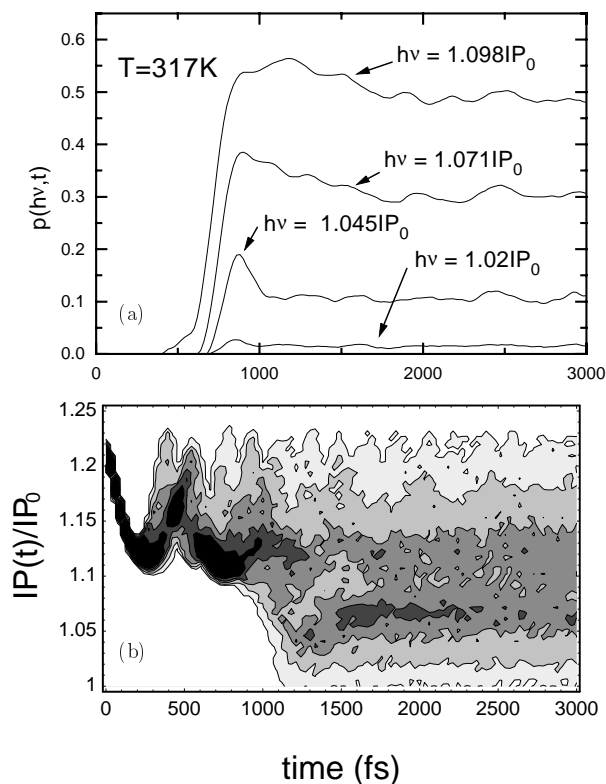
**Fig. 2a,b.** Temperature dependence of the inverse average fragmentation times $\langle \tau_F \rangle^{-1}$ for **a** Hg$_3^+$ and **b** Hg$_{13}^+$ clusters (*up triangles, left axis*) and rms bond-length fluctuations (*open circles, right axis*) $\delta$ before ionization for **a** Hg$_3$ and **b** Hg$_{13}$ clusters. Note that the increase in $\langle \tau_F \rangle^{-1}$ characterizes the melting temperature

**Fig. 1.** Calculated fragmentation-time distribution $W(t)$ for Hg$_6^+$ clusters at $T = 40$ K before ionization. Note that $W(t)$ also represents the probability of fragmentation per unit time

**Fig. 3.** Illustration of the optical excitation from a negatively charged to a neutral to a positively charged (NeNePo) silver trimer analyzed experimentally in [6]



**Fig. 4. a** Time dependence of the fraction of clusters $p(h\nu, t)$ with $IP(t)$ smaller than $h\nu$. The sharp increase and the overall time dependence of $p(h\nu, t)$ for increasing $h\nu$ should be compared with the experimental results of [6]. The initial temperature was $T = 317$ K. **b** Distribution of photodetached clusters as a function of time and IP for the same cluster ensemble as in **a**. *Black regions* indicate large number of clusters, whereas no clusters are present in the *white parts*. Note the progressive destruction of the coherent motion after photodetachment

*2.1.2 Response of* $Ag_3^-$ *clusters to ultrafast ionization.* The relaxation dynamics of an ensemble of silver trimers $Ag_3$ after photodetachment has been determined. At $t = 0$, due to the Franck–Condon principle, the clusters still retain their nearly linear shape, close to the ground-state structure of $Ag_3^-$. As the ground-state structure of $Ag_3$ corresponds to an obtuse isosceles triangle [14], the entire cluster ensemble finds itself in an extreme non-equilibrium situation, which leads to a very fast structural relaxation. In order to understand the experimental signal of [6], where a probe pulse ionizes all clusters with a structure close to the equilibrium structure of $Ag_3$, we calculate the ionization potential (IP) of the neutral silver trimers along their trajectories. The result is shown in Fig. 4b. In this contour plot, the number of clusters with a certain IP value is indicated by the grey scale, dark corresponding to high numbers of clusters. The IP is given relative to the value $IP_0$ which corresponds to $Ag_3$ in its equilibrium structure. The figure shows that all clusters of the ensemble start with IP values close to $1.2 IP_0$, indicating a nearly linear shape. Only after a relaxation time of 1 ps some of the clusters reach ionization potentials near $IP_0$, indicating a bent shape close to their equilibrium structure. Figure 4a now represents the ionization probability for the entire ensemble that can be deduced from Fig. 4b. Depending on the laser energy $h\nu$, a certain number of clusters with ionization potentials IP below $h\nu$ can be ionized, thus contributing to the experimental signal (yield of $Ag_3^+$). The curve corresponding to $h\nu = 1.045\ IP_0$ should be compared to the experimental result reported in [6]. $p(h\nu, t)$ displays the features observed in the experiment, namely first a sharp increase, then a maximum and finally a decrease to a smaller value, which remains constant. There is, however, a narrow range of frequencies $h\nu$, where the enhancement of the signal after the sharp increase is largest. For higher laser frequencies the maximum becomes broadened and the enhancement factor is smaller.

## 2.2 Moderate laser intensities. Pulses of finite duration

*2.2.1 Ultrafast dynamics of small* $Si_n$ *clusters.* We have studied the relaxation dynamics of laser-excited $Si_n$ clusters using the theory outlined in Sect. 1.2.1. The parameterization of the hopping integrals and the repulsive potential is taken from the work of Ho and coworkers [61]. The time step used for the molecular-dynamics simulation was $\Delta t = 0.05$ fs. We followed the time evolution of the clusters over a time interval $[0 : t_s]$ of 5 ps.

First we determined the ground-state geometries of the $Si_n$ clusters ($n = 2$–8) were determined by simulated annealing. Then we studied the ultrafast relaxation dynamics of these clusters upon excitation using laser pulses of different durations and for different values of the absorbed energies.

We obtain a significant dependence of the energy absorption and redistribution processes on the laser parameters (absorbed energy and duration). This fact suggests the construction for each cluster size of a generalized 'phase diagram', where the relaxation products ('phases') are plotted as a function of pulse duration and absorbed energy. If the relaxation process takes place in the form of structural changes (isomerization), then we consider the final state as belonging to the 'solid phase'. If melting-like behavior occurs as a consequence of the laser excitation, the final state is considered to be in the 'liquid phase'. Finally, if the relaxation process leads

to a fragmentation of the cluster, we consider the final state as belonging to the 'fragmented (gas) phase'. Since we investigate systems under extreme non-equilibrium conditions, the observed phases are not stationary but undergo an evolution in time. The $Si_5$ cluster, for example, may for certain laser parameters melt and at a later time fragment. Thus, the MD-simulation interval plays a decisive role in the characterization of the points in the phase diagrams. We used a time interval $[0 : t_s]$ of 5 ps. Test calculations for selected values of the laser parameters show that no dramatic energy redistributions occur beyond this time. This means that after 5 ps a considerable thermalization of the cluster has taken place and we expect the coexistence lines between the solid–liquid and solid–gas phases to remain almost unchanged if the simulation interval is increased. However, the liquid–gas transition line should further depend on $t_s$ due to the occurrence of statistical fragmentation.

We determine the solid–liquid-transition time by determining the jump of the mean square bonding length fluctuation $\delta$.

First, we determine the separation line between the fragmented and the non-fragmented phase by monitoring the bond lengths. Then, and in order to distinguish between liquid-like and solid-like, $\delta$ was calculated as a function of the laser parameters and separated into two regions corresponding to $\delta < 0.15$ and $\delta > 0.15$. The area lying between the line $\delta = 0.15$ (Lindemann criterion) and the line delimiting the fragments characterizes the liquid phase. The remaining area belongs to the solid phase (expansions and structural changes).

Figure 5 displays such 'phase diagrams' for $Si_5$ in a range of very short pulse durations. Both diagrams show the same feature: a liquid phase is only observed for pulse durations $\tau < 30$ fs. For longer pulses, the transition occurs directly from the solid to the fragmented phase.

For even longer durations and larger intensities we observe the following behavior: at fixed pulse energies short pulses produce more fragmentation than long pulses [55]. Such dependence of the fragmentation behavior on the pulse
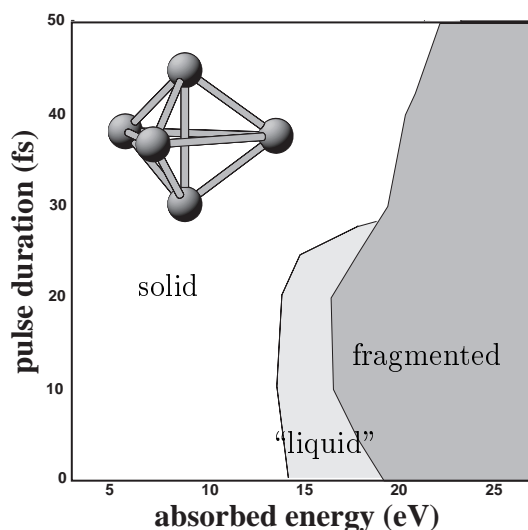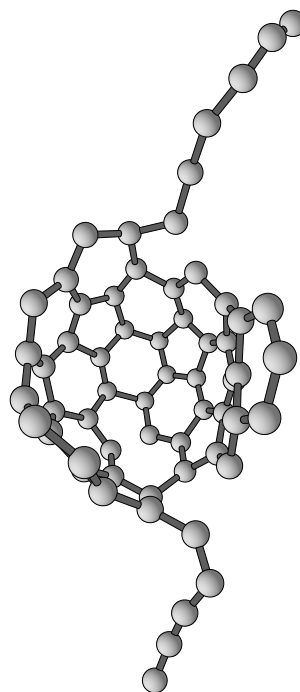
duration has also been observed in experiments using intense laser pulses [22].

*2.2.2 Ultrafast dynamics of* $C_{60}$ *and* $Si_{200}$. The laser-induced fragmentation of $C_{60}$ clusters was studied for a wide range of laser intensities and durations. In Fig. 6 a snapshot from the laser-induced fragmentation of a $C_{60}$ molecule is shown. Before the application of the laser pulse, the cluster was heated to a temperature of $T = 300$ K by simulated annealing. The laser pulse with a Gaussian envelope had a duration of 20 fs. The cluster absorbed an energy of 2.0 eV per atom. This energy is only slightly above the fragmentation threshold which was determined to be 1.9 eV/atom. The fragmentation mechanism that can be observed in Fig. 6 is a tearing of C–C bonds along one side of the molecule. Atoms with high kinetic energy form linear carbon chains dangling from both sides of the cluster. When these chains are 8 to 10 atoms in length, they tear themselves free from the main fragment. Note that this fragmentation mechanism is mainly observed for very short laser pulses, which are between 5 and 50 fs in duration, while for longer pulses (100 to 500 fs pulses were applied), the dominant fragmentation mechanism is the evaporation of very few atoms, which only much later leads to a further decay of the damaged fullerene molecule.

The changes in the vibrational modes of large silicon clusters due to a laser-induced electron–hole plasma were studied for the example of a $Si_{200}$ cluster. This cluster was prepared in close analogy to the formation of silicon clusters in the gas phase. Beginning from a nucleus of 3 silicon atoms, new single atoms were attached from random directions. In this process, positions which allowed the formation of two or even three bonds were favored over positions where only one bond

**Fig. 5.** Generalized 'phase diagram' (see text) for the products of the laser excitation (solid-like, liquid-like and fragmented clusters) as a function of the pulse duration and absorbed energy for $Si_5$

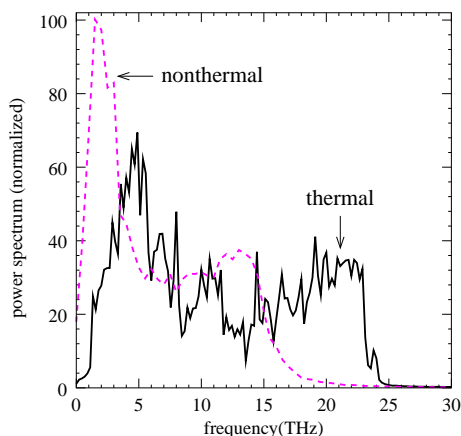**Fig. 6.** Snapshot of the laser fragmentation of a $C_{60}$ molecule. During a 20 fs laser pulse, 2.0 eV per atom was absorbed. In the figure, the molecule is shown 700 fs after the pulse maximum. Note that the spherical $C_{60}$ molecule has been torn open, with chains forming on two sides

**Fig. 7.** Power spectra of a Si$_{200}$ cluster. The *continuous line* corresponds to a thermal cluster at a temperature of $T = 300$ K, while the *dashed line* represents the spectrum of a cluster that absorbed 1.6 eV per atom during an 80 fs laser pulse (non-thermal cluster). Note the weight that is shifted from higher to lower frequencies as a consequence of the electron–hole plasma

could have been formed. After a new atom had been attached, the cluster was equilibrated for several hundred femtoseconds in order to allow structural relaxation. In this way, a cluster which is reasonably close to the equilibrium structure of Si$_{200}$ was formed. By simulated annealing, the cluster was heated to a temperature of $T = 300$ K. In Fig. 7, the power spectrum of this cluster at $T = 300$ K is shown as a continuous line. Subsequently, a trajectory of the Si$_{200}$ cluster following the action of an ultrashort laser pulse of medium intensity was calculated. During the pulse of 80 fs duration, 1.6 eV per silicon atom was absorbed by the cluster. After thermalization of the excited electrons, this leads to an electron temperature of $T_{el} = 18\,500$ K. The power spectrum corresponding to

this cluster trajectory is shown in Fig. 7 as a dashed line. In comparison to the power spectrum of the thermal-equilibrium trajectory, weight is transferred from high frequencies in the range of 15 to 25 THz to low frequencies. This can be understood as an effect of the electron–hole plasma: electrons that are excited into antibonding states weaken the overall bonding of the silicon cluster, which thus shifts vibrational modes towards lower frequencies. Note that a power spectrum calculated at an elevated equilibrium temperature of $T = 1100$ K closely resembles the spectrum of the $T = 300$ K trajectory; meanwhile, other power spectra calculated for non-equilibrium conditions at lower laser fluences and durations in comparison to the dashed line of Fig. 7 (laser duration 20 fs, absorption 0.8 and 1.3 eV/atom, respectively) confirm the above-mentioned observations on the power spectrum in the presence of an electron–hole plasma.

### 2.3 High laser intensities. Coulomb explosion

Our calculations describe a pulse with central wavelength $\lambda = 800$ nm and a Gaussian envelope. The maximal peak intensity has been chosen to be $3.7 \times 10^{16}$ W/cm$^2$. The duration of the pulse is 80 fs. In Fig. 8 we show four snapshots corresponding to different stages of the relaxation dynamics of Xe$_{20}$ after laser excitation. The first snapshot corresponds to the initial state. The second snapshot shows the initial stage in the ionization of the cluster. Note that nuclei remain in their initial positions. The third snapshot shows already a significant ionization of the cluster. The laser-induced motion of the electrons leads, through the electron–nuclei interactions, to collisions between the nuclei. The last snapshot displays a latter stage of cluster explosion, when a significant fraction of electrons have left the cluster and the internuclear distance rapidly increases, indicating the explosion of the cluster.
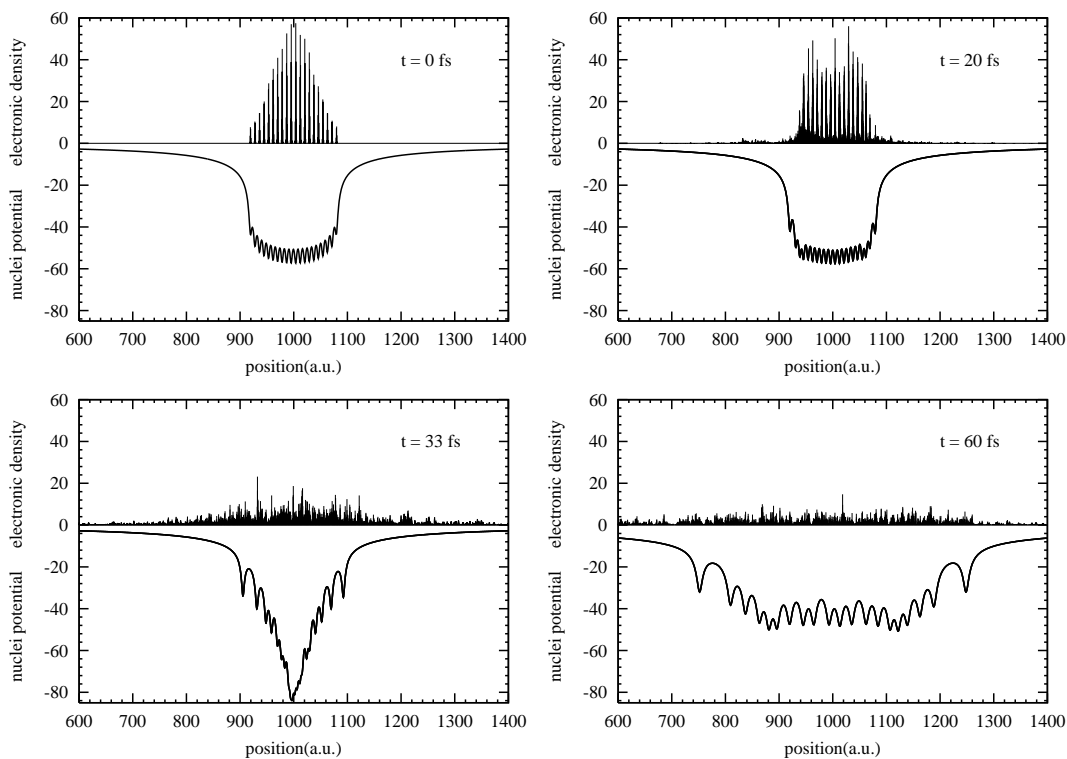


**Fig. 8.** Snapshots of the exploding Xe$_{20}$ at times $t = 0, 20, 35, 60$ fs for laser intensity of $3.7 \times 10^{16}$ W/cm$^2$ and 80 fs duration. The *thick line* refers to the ionic potential, whereas the *thin line* displays the electronic density
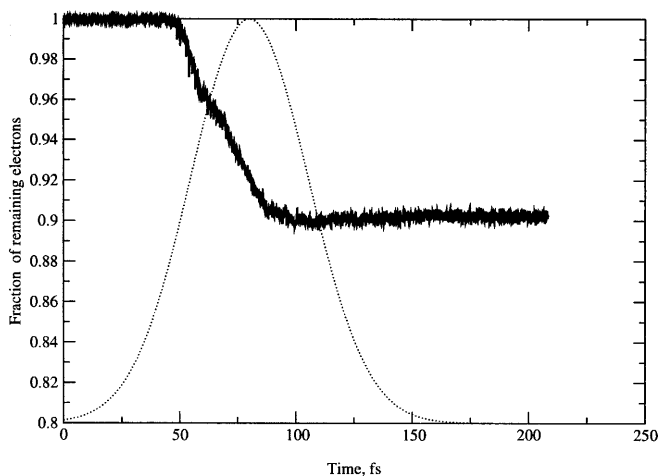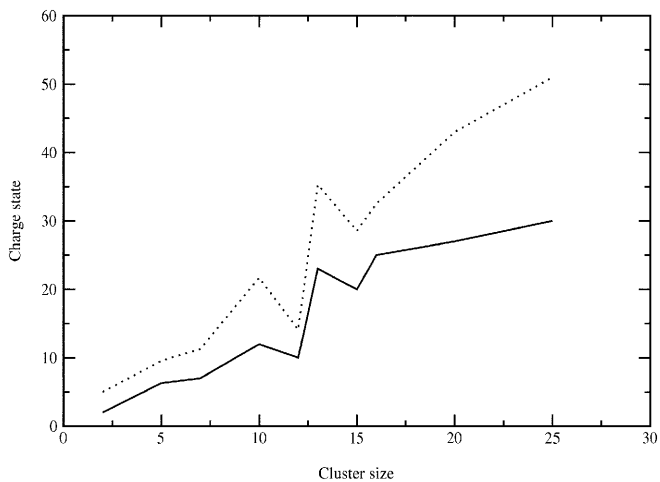
**Fig. 9.** Time dependence of the ionization process. Fraction of the total number of electrons in the cluster as a function of time for $Xe_5$. The atomic coordinates have been assumed to remain fixed. The *dotted line* displays the envelope function of the laser pulse, which has been shifted upwards for the sake of comparison

In Fig. 9 we show the time dependence of the ionization process. In this case we have assumed the nuclei to remain fixed at their initial positions throughout the electron dynamics. Note that the ionization process starts at the beginning of the laser pulse and comes to saturation when the intensity of the pulse reaches the maximum value. Figure 10 shows the average and maximal charge states of ions after explosion as function of cluster size. Note significant increasing of the maximal charge of ions with increasing of the cluster size. Upon excitation of large clusters, ions with a charge state $q > 40$ are present in our calculations, in qualitative agreement with experiment.

## 3 Summary

In this paper we have presented model calculations for the ultrafast dynamics of clusters in response to femtosecond laser pulses. We analyzed the different behavior of the relaxation dynamics of the clusters for different laser intensities. We presented different theoretical models for the description of the cluster dynamics in the different intensity regimes. We found that for low, moderate and high intensities different effects appear, going from interesting interplay between thermodynamics and short-time dynamics for low intensities, remarkable dependence of the dynamics of clusters on the pulse duration for moderate intensities, and highly charged ions as a product of the interaction of clusters with very intense laser fields.



**Fig. 10.** Dependence on the initial cluster size $n$ of the average (*solid line*) and maximal (*dotted line*) charge states of ions after explosion of $Xe_n$ clusters. The intensity of the laser pulse is $3.7 \times 10^{16}$ W/cm$^2$ and its duration 80 fs

## References

1. A. Zewail: *Femtosecond Chemistry*, Vol. 2 (Verlag Chemie, Heidelberg 1995) Chapt. 2
2. J. Manz, L. Wöste (Eds.): *Femtosecond Chemistry*, Vol. 1 (Verlag Chemie, Heidelberg 1995)
3. T. Baumert, R. Thalweiser, V. Weiss, E. Wiedemann, G. Gerber: Proc. of the Royal Netherlands Academy Colloquium on *Femtosecond Reaction Dynamics*, ed. by D.A. Wiersma **42**, 29 (1994)
4. T. Baumert, C. Röttgermann, C. Rothenfußer, R. Thalweiser, V. Weiss, G. Gerber: Phys. Rev. Lett. **69**, 1512 (1992)
5. I. Bañares, T. Baumert, M. Bergt, B. Kiefer, G. Gerber: Chem. Phys. Lett. **267**, 141 (1997)
6. S. Wolf, G. Sommerer, S. Rutz, E. Schreiber, T. Leisner, L. Wöste, R.S. Berry: Phys. Rev. Lett. **74**, 4177 (1995)
7. H. Kühling, K. Kobe, S. Rutz, E. Schreiber, L. Wöste: J. Phys. Chem. **97**, 12 500 (1993)
8. D.W. Boo, Y. Ozaki, L.H. Andersen, W.C. Lineberger: J. Phys. Chem. A **101**, 6688 (1997)
9. H. Haberland: Surf. Sci. **156**, 305 (1985)
10. M.E. Garcia, G.M. Pastor, K.H. Bennemann: Phys. Rev. B **48**, 8388 (1993); M.E. Garcia, G.M. Pastor, K.H. Bennemann: Z. Phys. D **26**, 293 (1993)
11. W. Kamke, J. de Vries, J. Krauss, E. Kaiser, B. Kamke, I.V. Hertel: Z. Phys. D **14**, 339 (1989)
12. U. Buck, H. Meyer: Phys. Rev. Lett. **52**, 109 (1984); D. Kreisle, O. Echt, M. Knapp, E. Recknagel: Phys. Rev. A **33**, 768 (1986)
13. V. Bonacic-Koutecky, L. Cespiva, P. Fantucci, J. Koutecky: J. Chem. Phys. **98**, 7981 (1993)
14. V. Bonacic-Koutecky, L. Cespiva, P. Fantucci, J. Pittner, J. Koutecky: J. Chem. Phys. **100**, 490 (1994)
15. C.V. Shank, R. Yen, C. Hirlimann: Phys. Rev. Lett. **51**, 900 (1983)
16. H.W.K. Tom, G.D. Aumiller, C.H. Brito-Cruz: Phys. Rev. Lett. **60**, 1438 (1988)
17. K. Sokolowski-Tinten, J. Bialkowski, D. von der Linde: Phys. Rev. B **51**, 14 186 (1995)
18. P. Stampfli, K.H. Bennemann: Phys. Rev. B **42**, 7163 (1990)
19. P. Stampfli, K.H. Bennemann: Phys. Rev. B **49**, 7299 (1994)
20. P.L. Silvestrelli, A. Alalvi, M. Parrinello, D. Frenkel: Phys. Rev. Lett. **77**, 3149 (1996)
21. V. Blanchet, C. Nicole, M.-A. Bouchene: Phys. Rev. Lett. **78**, 2716 (1996)
22. B. Bescós, R. Hoch, H.-J. Schmidtke, G. Gerber: Appl. Phys. B **71**, 373 (2000)
23. See for example T.L. Beck, J. Jellinek, R.S. Berry: J. Chem. Phys. **87**, 545 (1987)
24. M.E. Garcia, G.M. Pastor, K.H. Bennemann: Phys. Rev. Lett. **67**, 1142 (1991)
25. M.E. Garcia, K.H. Bennemann: Comput. Mater. Sci. **2**, 481 (1994)
26. H. Haberland, H. Kornemeier, H. Langosch, M. Oschwald, G. Tanner: J. Chem. Soc., Faraday Trans. **86**, 2473 (1990)
27. K. Rademann, B. Kaiser, U. Even, F. Hensel: Phys. Rev. Lett. **59**, 2319 (1987)
28. E.M. Snyder, S.A. Buzza, A.W. Castleman: Phys. Rev. Lett. **77**, 3347 (1996)
29. D. Normand, M. Schmidt: Phys. Rev. A **53**, R1958 (1996)
30. Y.L. Shao, T. Ditmire, J.W.G. Tisch, E. Springate, J.P. Marangos, M.H.R. Hutchinson: Phys. Rev. Lett. **77**, 3343 (1996)

31. T. Ditmire, J.W.G. Tisch, E. Springate, M.B. Mason, N. Hay, R.A. Smith, J.P. Marangos, M.H.R. Hutchinson: Nature (London) **386**, 54 (1997)

32. T. Ditmire, T. Donnelly, A.M. Rubenchik, R.W. Falcone, M.D. Perry: Phys. Rev. A **53**, 3379 (1996)

33. T. Ditmire, J.W.G. Tisch, E. Springate, M.B. Mason, N. Hay, J.P. Marangos, M.H.R. Hutchinson: Phys. Rev. Lett. **78**, 2732 (1997)

34. L. Köller, M. Schumacher, J. Köhn, S. Teuber, J. Tiggesbäumker, K.H. Meiwes-Broer: Phys. Rev. Lett. **82**, 3783 (1999)

35. A. McPherson, B.D. Thomson, A.B. Borisov, K. Boyer, C.K. Rhodes: Nature (London) **370**, 631 (1994)

36. T. Donnelly, T. Ditmire, K. Neuman, M.D. Perry, R.W. Falcone: Phys Rev. Lett. **76**, 2472 (1996)

37. M. Lezius, S. Dobosz, D. Normand, M. Schmidt: Phys. Rev. Lett. **80**, 261 (1998)

38. F. Calvayrac, P.G. Reinhard, E. Suraud: J. Phys. B **31**, 5023 (1998)

39. M.E. Garcia, D. Reichardt, K.H. Bennemann: J. Chem. Phys. **107**, 9857 (1997)

40. M.E. Garcia, D. Reichardt, K.H. Bennemann: J. Chem. Phys. **109**, 1101 (1998)

41. F.Yu. Naumkin, P.J. Knowles, J.N. Murrell: Chem. Phys. **193**, 27 (1995); P.J. Knowles, J.N. Murrell: Molec. Phys. **87**, 827 (1996)

42. P.J. Kuntz, J. Valldorf: Z. Phys. D **8**, 195 (1988)

43. M. Amarouche, G. Durand, J.P. Malrieu: J. Chem. Phys. **88**, 1010 (1988)

44. H.U. Böhmer, S.D. Peyerimhoff: Z. Phys. D **11**, 239 (1989)

45. D. Reichardt, M.E. Garcia, K.H. Bennemann: Surf. Rev. Lett. **3**, 567 (1996)

46. L. Goodwin, A.J. Skinner, D.G. Pettifor: Europhys. Lett. **9**, 701 (1989)

47. J.C. Slater, G.F. Koster: Phys. Rev. **94**, 1498 (1954)

48. L. Verlet: Phys. Rev. **159**, 98 (1967)

49. C. Moore: Atomic Energy Levels, Nat. Bur. Stand. Circ. No. 467 (1958)

50. W.A. Harrison: Phys. Rev. B **24**, 5835 (1981)

51. J. Ho, K.M. Erwin, W.C. Lineberger: J. Chem. Phys. **93**, 6987 (1990)

52. W.H. Knox, D.S. Chemla, G. Livescu, J.E. Cunningham, J.E. Henry: Phys. Rev. Lett. **61**, 1290 (1988)

53. D. Agassi: J. Appl. Phys. **55**, 4376 (1984)

54. C.A. Ullrich, P.-G. Reinhard, E. Suraud: J. Phys. B **31**, 1871 (1998)

55. K. Zickfeld, M.E. Garcia, K.H. Bennemann: Phys. Rev. B **59**, 13 422 (1999)

56. K. Zickfeld: Diploma Thesis, Freie Universität Berlin (1998)

57. H.O. Jeschke, M.E. Garcia, K.H. Bennemann: Phys. Rev. B **60**, R3701 (1999)

58. J. Javanainen, H.H. Eberly, Q. Su: Phys. Rev. A **38**, 3430 (1996)

59. M. Brewczyk, K. Rzazewski, C.W. Clark: Phys. Rev. A **52**, 1468 (1995); K.C. Kulander, F.H. Mies, K.J. Schafer: Phys. Rev. A **53**, 2562 (1996)

60. M. Brewczyk, C.W. Clark, M. Lewenstein, K. Rzazewski: Phys. Rev. Lett. **80**, 1857 (1998)

61. I. Kwon, R. Biswas, C.Z. Wang, K.M. Ho, C.M. Soukoulis: Phys. Rev. B **49**, 7242 (1994)